Downloaded from orbit.dtu.dk on: Apr 26, 2024

DTU Library

Compact dual-strain sensitivity polymer optical fiber grating for multi-parameter sensing

Pereira, Luis; Min, Rui; Paixao, Tiago; Marques, Carlos; Woyessa, Getinet; Bang, Ole; Pinto, Joao Lemos; Antunes, Paulo

Published in:
Journal of Lightwave Technology

Link to article, DOI:
10.1109/JLT.2020.3046077

Publication date:
2021

Document Version
Peer reviewed version

Link back to DTU Orbit

Citation (APA):
Pereira, L., Min, R., Paixao, T., Marques, C., Woyessa, G., Bang, O., Pinto, J. L., & Antunes, P. (2021). Compact dual-strain sensitivity polymer optical fiber grating for multi-parameter sensing. *Journal of Lightwave Technology*, *39*(7), 2230-2240. https://doi.org/10.1109/JLT.2020.3046077

General rights
Copyright and moral rights for the publications made accessible in the public portal are retained by the authors and/or other copyright owners and it is a condition of accessing publications that users recognise and abide by the legal requirements associated with these rights.

- Users may download and print one copy of any publication from the public portal for the purpose of private study or research.
- You may not further distribute the material or use it for any profit-making activity or commercial gain
- You may freely distribute the URL identifying the publication in the public portal

If you believe that this document breaches copyright please contact us providing details, and we will remove access to the work immediately and investigate your claim.

This article has been accepted for publication in a future issue of this journal, but has not been fully edited. Content may change prior to final publication. Citation information: DOI 10.1109/JLT.2020.3046077, Journal of Lightwave Technology

Compact dual-strain sensitivity polymer optical fiber grating for multi-parameter sensing

Luís Pereira, Rui Min, Tiago Paixão, Carlos Marques, Getinet Woyessa, Ole Bang, João L. Pinto, and Paulo Antunes

***Abstract*— In this paper, two configurations are presented for simultaneous measurement of strain and temperature by reducing the cross-section area in small regions of the fiber where the Bragg gratings were inscribed, to achieve dual sensitivity to strain and handle the cross-sensitivity to temperature of a single grating. Each configuration used a single Bragg grating inscribed in a 2-ring undoped *poly (methyl methacrylate)* microstructured polymer optical fiber (mPOF) with a pulsed Q-switched Nd:YAG laser system. To reduce the cross-section area, a femtosecond laser system was used to remove portions of the mPOF, creating micromachined slots in the fiber, with different lengths for each configuration. The result was the appearance of a second peak when strain is applied, with a higher strain sensitivity. The thermal, humidity and refractive index response of these gratings were analyzed, revealing a thermal sensitivity almost twice the value of a common Bragg grating inscribed in the same mPOF. The maximum root mean square errors obtained when both strain and temperature are applied in these grating devices were 52 με and 0.6 ºC, respectively. These results show that the method used to produce these devices could be a suitable and reliable option to fabricate very compact sensors to simultaneously measure strain and other parameters, such as temperature. Moreover, these devices may be used as phase-shift gratings since the position of the reflective peaks and their relative spectral separation may be modulated by applying strain to the optical fiber.**

***Index Terms*—Fiber gratings, Optical fiber sensors, Plastic optical fiber, Dual sensitivity.**

I. Introduction

POLYMER optical fibers (POFs) present unique and interesting properties which allow its use in different applications in the sensing field. The lower Young´s modulus and higher elastic strain limits [1]-[3] comparing with silica fibers, enable POFs to be applied as strain [4],[5], stress [6], bending [7], acceleration [8] or pressure sensors [9]. Among other advantageous properties, POFs have a negative thermo-optic coefficient and high sensitivity to temperature [10], exhibit excellent compatibility with organic materials which confers great potential for biomedical applications [11], and some materials, such as the *poly(methyl methacrylate)* (PMMA), have affinity to water [12], allowing to monitor humidity based parameters.

The first fiber Bragg gratings (FBGs) in POF were inscribed in 1999 by Peng et al [13], using two illumination wavelengths, 248 nm and 325 nm, to create different gratings. Since then, both wavelengths have been heavily used to manufacture polymer optical fiber Bragg gratings (POFBGs). The HeCd laser operating at 325 nm is an affordable and accessible equipment, being the preferred option to avoid any ablation issues due to high pulse energy [14], and to obtain deeper penetration of the radiation on the material [15]. On the other hand, the KrF laser operating at 248 nm allows to decrease the POFBG inscription time [16]-[18] due to the higher absorption of the polymer materials (such as PMMA) for shorter wavelengths. POFBGs inscription in different materials such as PMMA [12],[19], Topas [20],[21], Zeonex [22],[23], polycarbonate [24]-[26] and CYTOP [27],[28] have been reported, allowing to take advantage of their unique characteristics for sensing purposes. As most polymers are intrinsically photosensitive to UV light, FBG inscription in different polymers is possible without doping [23]. However, the fabrication of Bragg gratings in undoped POFs can be a time consuming process, and that time can easily increase for

This paragraph of the first footnote will contain the date on which you submitted your paper for review.

This work was developed within the scope of the project I3N UIDB/50025/2020 and UIDP/50025/2020, financed by national funds through the Fundação para a Ciência e a Tecnologia (FCT)/MEC. Carlos Marques acknowledges FCT through the CEECIND/00034/2018 (iFish project). The work of Luís Pereira and Tiago Paixão was also supported by FCT under the grant with references SFRH/BD/146295/2019 and PD/BD/128265/2016, respectively. The work of Rui Min was supported by National Natural Science Foundation of China (62003046).

L. Pereira, T. Paixão, C. Marques, and J. L. Pinto are with the I3N & Physics Department of the University of Aveiro, 3810-193, Aveiro, Portugal (e-mail: lmpereira@ua.pt; tiagopaixao@ua.pt; carlos.marques@ua.pt; jlp@ua.pt).

R. Min is with the Center for Cognition and Neuroergonomics, State Key Laboratory of Cognitive Neuroscience and Learning, Beijing Normal University at Zhuhai 519087, China (e-mail: rumi@alumni.upv.es).

G. Woyessa is with the DTU Fotonik, Department of Photonics Engineering, Technical University of Denmark, Denmark (e-mail: gewoy@fotonik.dtu.dk).

O. Bang is with the DTU Fotonik, Department of Photonics Engineering, Technical University of Denmark, and SHUTE Sensing Solutions A/S, Oldenvej 1A, 3490 Kvistgaard, Denmark (e-mail: oban@fotonik.dtu.dk).

P. Antunes is with the Instituto de Telecomunicações and I3N & Physics Department of the University of Aveiro, 3810-193, Aveiro, Portugal (e-mail: pantunes@ua.pt).

0733-8724 (c) 2020 IEEE. Personal use is permitted, but republication/redistribution requires IEEE permission. See http://www.ieee.org/publications_standards/publications/rights/index.html for more information.
Authorized licensed use limited to: Danmarks Tekniske Informationscenter. Downloaded on January 06,2021 at 06:06:43 UTC from IEEE Xplore. Restrictions apply.

This article has been accepted for publication in a future issue of this journal, but has not been fully edited. Content may change prior to final publication. Citation information: DOI 10.1109/JLT.2020.3046077, Journal of Lightwave Technology

microstructured POFs (mPOFs) [29]. Using a high average power UV continuous (CW) beam from a HeCd laser system it is possible to obtain POFBGs in PMMA mPOFs in less than 7 minutes [29], and using a KrF laser system, that time can be less than 30 seconds [16],[26]. Also, point-by-point laser writing of gratings in mPOFs through femtosecond lasers has been achieved, with an inscription time around 2.5 seconds [30]. Regarding the Nd:YAG laser system at 266 nm radiation, POFBGs inscription in undoped PMMA-mPOF with different number of microstructured rings was achieved, with an inscription time of several minutes [31]. Doping the PMMA material with *benzildimethylketal* (BDK) to enhance the photosensitivity of the core can reduce the inscription time to few minutes in step index POFs and mPOFs, using 355 nm [32] and 325 nm [33] wavelength radiation, respectively. The inscription time can be reduced even further, to less than a second in mPOFs, using just a single pulse from both 248 nm [18],[34] and 266 nm wavelength radiation [35]. Nevertheless, the addition of dopants can introduce some drawbacks such as the significantly higher fiber price and transmission losses around 800 nm [36]. These disadvantages can be a critical issue for some real applications based on POF, making the undoped mPOF more suitable for low transmission loss applications.

Although FBGs are one of the most used and well-known structure in optical sensing, they have a major drawback regarding its inability to eliminate cross-sensitivity effects. Strain and temperature are usually the parameters where this effect must be addressed, but depending on the sensing application and fiber materials, other parameters (such as humidity and refractive index) may also take part on the cross-sensitivity effect. Several techniques have already been developed for simultaneous measurements in silica optical fibers, POFs and in configurations using both silica and polymer fibers. Most of these configurations rely on the use of 2 gratings with different sensitivity capabilities, which include the use of specific materials as coating in one grating or more [37]-[39], the use of a reference FBG to calibrate the response of the other FBG to a certain parameter [40],[41], splicing two fibers with different diameters where the gratings show different sensitivity to strain [42], producing 2 gratings in both etched and unetched areas in silica fiber [43] and POF [44],[45], using dual-grating in a fiber made of two different materials [23], and the combination of a POFBG and a single grating in silica fiber [46]. Regarding the use of a single FBG, some techniques have been demonstrated based on the application of coating materials covering just a section [47] or the entire grating [48]. Also, the use of chirped tapered FBGs may provide different sensitivities for strain and temperature [49],[50], together with other parameters (such as refractive index [51]) when variations in the spectral bandwidth are considered.

In order to overcome the cross-sensitivity effect on POFBGs, we report on a new technique based on a single POFBG. Two configurations are proposed, both showing dual-sensitive to strain by decreasing the optical fiber diameter of small sections where the POFBGs were inscribed. The results show great potential for the use of a single POFBG in simultaneous measurement applications. The fact that just one FBG can be used to monitor more than one parameter, without the application of other materials as coating or capsules, improves the possibility to create very small multiparameter sensors for *in-situ* applications in real scenarios.

II. Principle of Operation and Sensor Fabrication

A. Principle of Operation

The configuration of the proposed sensor is based on the use of a single POFBG, in which a section of the POF diameter is removed in the area where the grating was inscribed. The main objective is to reduce the cross-section area of the fiber (A) in that region by reducing the fiber diameter, in order to obtain dual sensitivity to strain by the same grating. The relationship between the strain sensitivity of the FBG and the Hooke´s Law is given by the following equation:

$$\frac{\Delta\lambda_B}{\lambda_B} = (1-\rho_e)\frac{F_z}{EA} \tag{1}$$

where λ_B and $\Delta\lambda_B$ are the Bragg wavelength and the Bragg wavelength variation, respectively, ρ_e and E are the effective photoelastic constant and the Young´s modulus of the fiber, respectively, and F_z is the longitudinal applied force. For a certain λ_B, and considering that ρ_e and E are constant for a specific fiber, the $\Delta\lambda_B$ depends on F_z and A. If F_z is constant along the fiber length, as A decreases, the $\Delta\lambda_B$ to strain will increase according to (1). Using this principle, the objective is to obtain for a single POFBG, different values of $\Delta\lambda_B$ with a single value of external force applied, resulting in different values of strain sensitivities. Then, strain and temperature changes ($\Delta\varepsilon$ and ΔT, respectively) can be simultaneously measured by using the following characterization matrix:

$$\begin{bmatrix}\Delta\varepsilon\\ \Delta T\end{bmatrix} = \frac{1}{K_{1\varepsilon}K_{2T} - K_{2\varepsilon}K_{1T}}\begin{bmatrix}K_{2T} & -K_{1T}\\ -K_{2\varepsilon} & K_{1\varepsilon}\end{bmatrix}\begin{bmatrix}\Delta\lambda_1\\ \Delta\lambda_2\end{bmatrix} \tag{2}$$

where K_{1T}, K_{2T} are the thermal sensitivities and $K_{1\varepsilon}$, $K_{2\varepsilon}$ are the strain sensitivities of a single POFBG.

B. POFBG Inscription and Experimental Setup

The optical fiber used to inscribe the POFBGs was a 2-ring undoped PMMA mPOF with a hexagonal hole structure (see Fig 1), manufactured at *DTU Fotonik* (Denmark). The average hole diameter and pitch in the fiber are 1.70 µm and 3.95 µm, respectively. The fiber has an outside diameter of 138 µm and an average core diameter of 6.2 µm, approximately. The low number of hexagonal rings in this mPOF facilitates the inscription of strong and stable gratings by UV radiation [31], and to simplify the POFBG interrogation, the mPOFs samples with a length of about 20 cm were glued to FC/PC connectors and cleaved with a special room temperature cleaver [52]. Then, the end face of the mPOF went through a polishing process to enhance the transmission quality, by removing the inherent defects associated with the cleaving process. Before the inscription, the mPOFs were pre-annealed during 24 hours at 70 ºC to reduce the internal stress in the fiber originated during the fabrication process, and to improve the POFBGs´ sensing performance [53],[54].

The inscription setup, based on the phase mask technique, is shown in Fig. 1. A pulsed Q-switched Nd:YAG laser system

0733-8724 (c) 2020 IEEE. Personal use is permitted, but republication/redistribution requires IEEE permission. See http://www.ieee.org/publications_standards/publications/rights/index.html for more information.
Authorized licensed use limited to: Danmarks Tekniske Informationscenter. Downloaded on January 06,2021 at 06:06:43 UTC from IEEE Xplore. Restrictions apply.

This article has been accepted for publication in a future issue of this journal, but has not been fully edited. Content may change prior to final publication. Citation information: DOI 10.1109/JLT.2020.3046077, Journal of Lightwave Technology

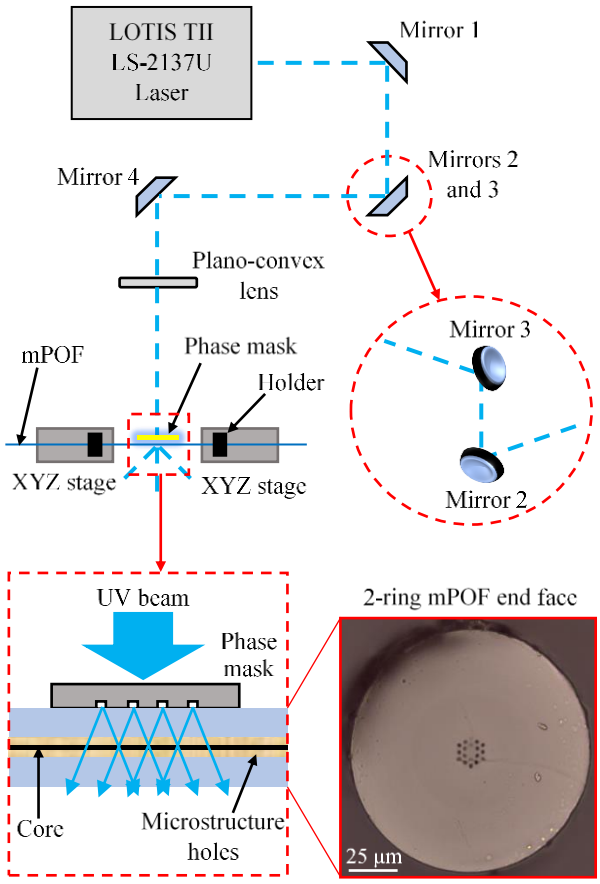

Fig. 1. Sketch of the experimental setup based on phase mask technique.

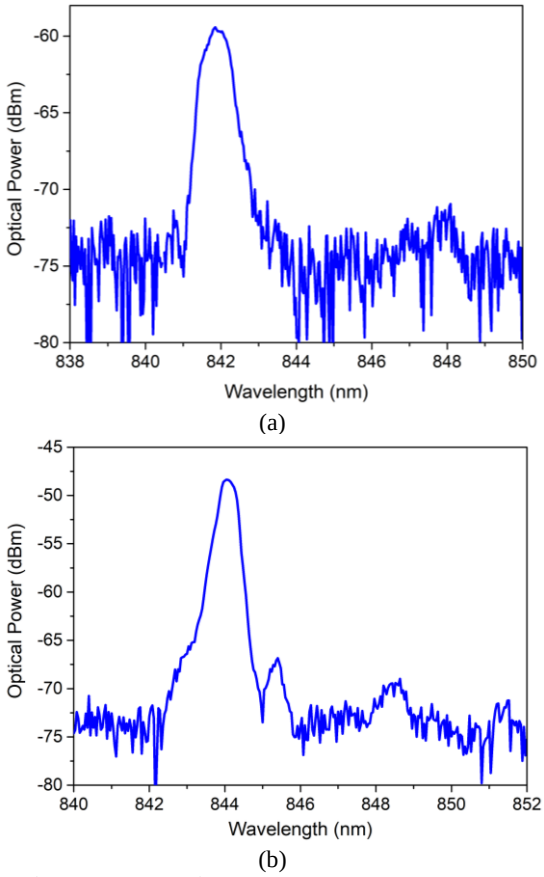

Fig. 2. Reflection spectrum after inscription: (a) POFBG 1. (b) POFBG 2.

(LOTIS TII LS-2137U Laser) lasing at the fourth harmonic (266 nm) was employed to produce the POFBGs. The laser beam profile is circular, the diameter is about 8 mm and the divergence ≤1.0 mrad. Before reaching the optical fiber, the laser beam is focused onto the fiber core by a plano-convex cylindrical lens with an effective focal length of 320 mm, originating an effective spot size on the fiber surface with about 8 mm in width and about 30 µm in height. The laser parameters employed were 24.6 J of pump energy with an 8 ns pulse repetition rate of 5 Hz. The phase mask has 10 mm in length surface relief structure, a period of Λ_{PM} = 567.8 nm, is designed to operate at 248 nm irradiation and produce gratings in PMMA mPOFs with a final λ_B around 844 nm. The grating spectrum was monitored in reflection, using a super luminescent diode (SUPERLUM SLD-mCS-371 Miniature Broadband Light Source Module), an optical spectrum analyzer (Anritsu, model MS9740A) and a 50:50 ratio SM-silica optical coupler.

Two gratings, with approximately 8 mm of physical length, were produced in different 2-ring undoped PMMA mPOF samples. The reflection spectrums of each POFBG after inscription are shown in Fig. 2. When placing the mPOFs at the inscription setup, a random pre-tension was applied manually to guarantee that they were fixed and positioned in parallel with the phase mask, which influenced the final value of λ_B for each POFBG. For POFBG 1, instead of getting a value of 844 nm for the λ_B, a value of 841.50 nm was achieved (see Fig. 2 (a)). The reflective signal of this grating has about 16 dB of peak power and the 3-dB bandwidth is approximately 870 pm. Regarding POFBG 2, the obtained value of λ_B was 844.06 nm, mainly due to the lack of mechanical tension applied when the POF was placed on the inscription setup. This grating has about 27 dB of reflective peak power and the 3-dB bandwidth is approximately 560 pm.

The growth rate of POFBG 1 during inscription was lower than POFBG 2, ceasing after 8 minutes of irradiation exposure, while POFBG 2 had an inscription time of 12 minutes. This grating inscription time difference can be explained by variations of the microstructure holes position regarding the laser path, which could generate laser scattering, thus affecting the energy density of the UV laser beam in the fiber core [55].

C. Cross-section Area Reduction by Femtosecond Laser

After the POFBGs production, they went through a femtosecond laser treatment in order to reduce the cross-section area in some specific sections of the gratings. Using high energy femtosecond laser pulses, portions of PMMA material were removed from the outermost region of the mPOFs. The experimental setup employed in this process is presented in Fig. 3, which is based on a femtosecond laser from Quantronix (λ=795 nm, pulse width ~ 130 fs and repetition rate of 1 kHz). The micromachined slots were produced by using a 3-axis motorized translation platform, where a x50 NIR microscope objective lens (with a NA value of 0.67 and a focal distance of 10 mm, from Optosigma) focused the laser beam on the POFs´ surface. To assist and visualize at real time the structures´ micromachining, a CCD camera was mounted on top of the setup, perpendicularly to the optical fiber and aligned with the laser beam. Each POF was mounted onto two holders and

0733-8724 (c) 2020 IEEE. Personal use is permitted, but republication/redistribution requires IEEE permission. See http://www.ieee.org/publications_standards/publications/rights/index.html for more information.
Authorized licensed use limited to: Danmarks Tekniske Informationscenter. Downloaded on January 06,2021 at 06:06:43 UTC from IEEE Xplore. Restrictions apply.

This article has been accepted for publication in a future issue of this journal, but has not been fully edited. Content may change prior to final publication. Citation information: DOI 10.1109/JLT.2020.3046077, Journal of Lightwave Technology

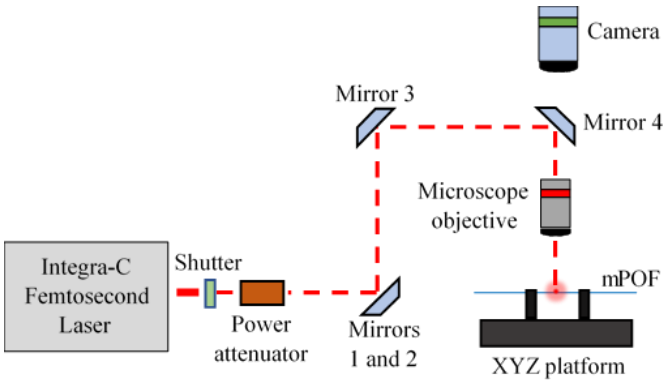

Fig. 3. Sketch of the experimental setup used to produce the micromachined slots.

aligned with the laser beam by the camera and the 3-axis motorized platform. The laser beam power used was 3.3 mW (measured before the microscope objective lens), and the POF was moved perpendicularly to the laser beam at a constant velocity of 0.3 mm/s.

The laser beam after passing through the microscope objective is focused on a spot with, approximately, 2 µm of diameter. This spot was positioned at 5 µm from the POF surface, and moved along two pre-selected fiber lengths, removing about 5 µm height of material from the POFs. Each POFBG went through 4 sweeps in opposite sides of the fiber, removing about 20 µm of polymer material in depth in each side, as showed in Fig. 4. The cross-section area was reduced by approximately 18% in both POFBGs. In POFBG 1, the length of the micromachined slot is approximately 250 µm (see Fig. 4 (a)) and its location is close to the center of the grating, while in POFBG 2 the length is approximately 4 mm (see Fig. 4 (b)) and covers, approximately, half the grating length.

After fabricating the micromachined slots, the POFBGs spectra were monitored to analyze any changes caused by the slots production and femtosecond laser irradiation. Fig. 5 shows the spectra from both POFBGs before and after the micromachined slots production. The spectra from POFBG 1, depicted in Fig 5 (a), show a phase-shift effect after the slots production. This phase-shift could be related to a residual applied strain on the POF during the micromachining process, which after this process is concluded results in a drift of the original POFs elastic structure without any applied strain, creating a phase offset between the two halves of the POFBG. However, 1 day after the slot production, the POFBG 1 spectrum returned to the same spectral characteristics as it had before the slot fabrication, showing the inexistence of a permanent elastic deformation on the POFBG. Regarding POFBG 2, the spectra, before and right after the slots production, are very similar, revealing the inexistence of elastic deformation in the treated section of the fiber (see Fig 5 (b)).

III. Sensing Performance

A. *Strain Response*

The individual strain response of the POFBGs was studied to analyze the grating stability and sensing properties. As mentioned before, two portions of a POFBG with different cross-section areas cause a dual-response of the grating when

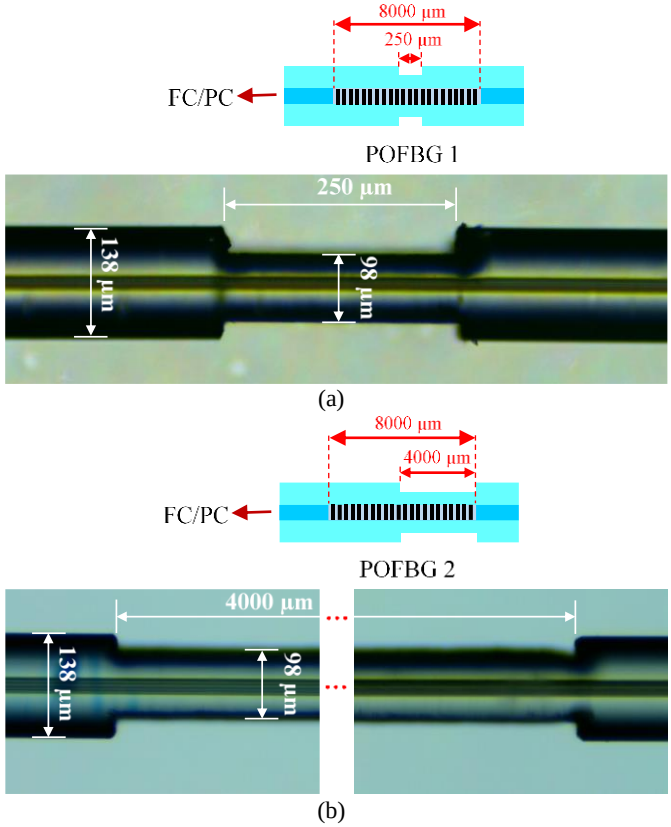

Fig. 4. Schematic representations and microscopic images of the micromachined slots: (a) POFBG 1. (b) POFBG 2.

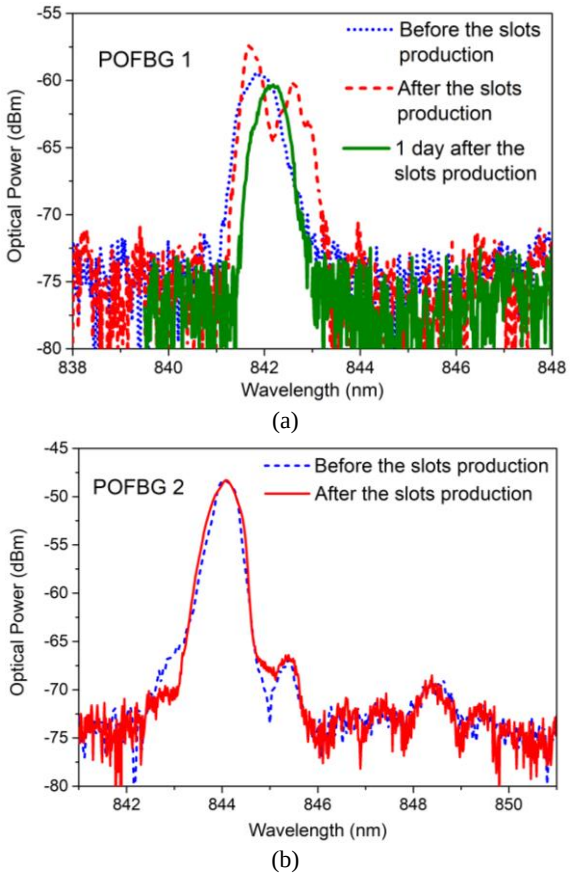

Fig. 5. Reflection spectra before and after the micromachined slots production: (a) POFBG 1. (b) POFBG 2.

0733-8724 (c) 2020 IEEE. Personal use is permitted, but republication/redistribution requires IEEE permission. See http://www.ieee.org/publications_standards/publications/rights/index.html for more information.
Authorized licensed use limited to: Danmarks Tekniske Informationscenter. Downloaded on January 06,2021 at 06:06:43 UTC from IEEE Xplore. Restrictions apply.

This article has been accepted for publication in a future issue of this journal, but has not been fully edited. Content may change prior to final publication. Citation information: DOI 10.1109/JLT.2020.3046077, Journal of Lightwave Technology

strain is applied to it, since the $\Delta\lambda_B$ is different for each section. The strain characterization was performed by fixing the fibers between a fixed and a manual 3-axis translation stage, with 1 μm resolution. Both POFBGs went through 3 testing cycles of strain response analysis, where increasing and decreasing strain regimes were applied. In order to analyze the hysteresis effect, the fiber was stretched up to different relative strain values in each cycle (up to 3430 με, 5480 με and 6850 με in cycle 1, cycle 2 and cycle 3, respectively), with steps around 690 με and a stabilization time of 5 minutes.

The reflection spectra and the corresponding response of the POFBGs 1 and 2 during the cycle 2 for different percentages of applied strain are shown in Fig. 6. During the increasing strain regime, a second reflected peak (peak 2) with different response from the original Bragg wavelength peak (peak 1), appears above a relative applied strain of 690 με and 960 με in POFBG 1 (see Fig. 6 (a)) and POFBG 2 (see Fig. 6 (c)), respectively. In POFBG 1, the wavelength shift of both peaks for cycle 2 is presented in Fig. 6 (b), and the obtained strain sensitivities for peak 1 were 0.78 ± 0.01 pm/με (increasing strain) and 0.77 ± 0.02 pm/με (decreasing strain). Regarding peak 2, the obtained sensitivities were 1.47 ± 0.03 pm/με and 1.44 ± 0.03 pm/με for increasing and decreasing strain, respectively, which is almost twice the sensitivity values of peak 1. The POFBG 2 showed a behavior similar to POFBG 1 when strain was applied. The displacement of both peaks with increasing and decreasing strain during cycle 2 is presented in Fig. 6 (d). The obtained sensitivities for peak 1 were 0.72 ± 0.01 pm/με (increasing strain) and 0.70 ± 0.01 pm/με (decreasing strain), and for peak 2 were 1.30 ± 0.03 pm/με (increasing strain) and 1.23 ± 0.04 pm/με (decreasing strain).

To analyze hysteresis effect, two more testing cycles were performed to maximum relative strain values of 3430 με and 6850 με. Table I shows the strain sensitivities of peak 1 and peak 2 during the 3 cycles for increasing/decreasing strain and the respective maximum hysteresis level. The lowest coefficient of determination (R^2) obtained in the strain response of both grating devices was 0.9949. Cycle 1, where the strain was increased up to 3430 με, shows the lowest hysteresis level for peak 2 in both POFBGs, getting higher as the strain increases to 5480 με (cycle 2) and 6850 με (cycle 3). As the maximum applied strain increases, the relation stress-strain gets closer to the yield point (limit of the elastic behavior), which can explain the increasing hysteresis. Since there is a section of the POFBGs with lower diameter and higher stress, for the same applied force, the amount of strain is higher in that region and consequently is closer to the yield point when compared with the rest of the fiber. These results show that these POFBGs are more suitable to monitor low values of strain where both peaks present good responses with low hysteresis level.

B. Temperature Response

The temperature response of both devices was measured by using a custom tubular furnace, with 1 °C resolution. The temperature was initially increased from 25 ºC to 45 ºC, and later decreased back to 25 ºC, by steps of 5 ºC. In each step, the temperature was kept constant over 30 minutes to ensure thermal stabilization. Fig. 7 (a) and 7 (c) show the reflection spectra of POFBG 1 and POFBG 2 under 2 different

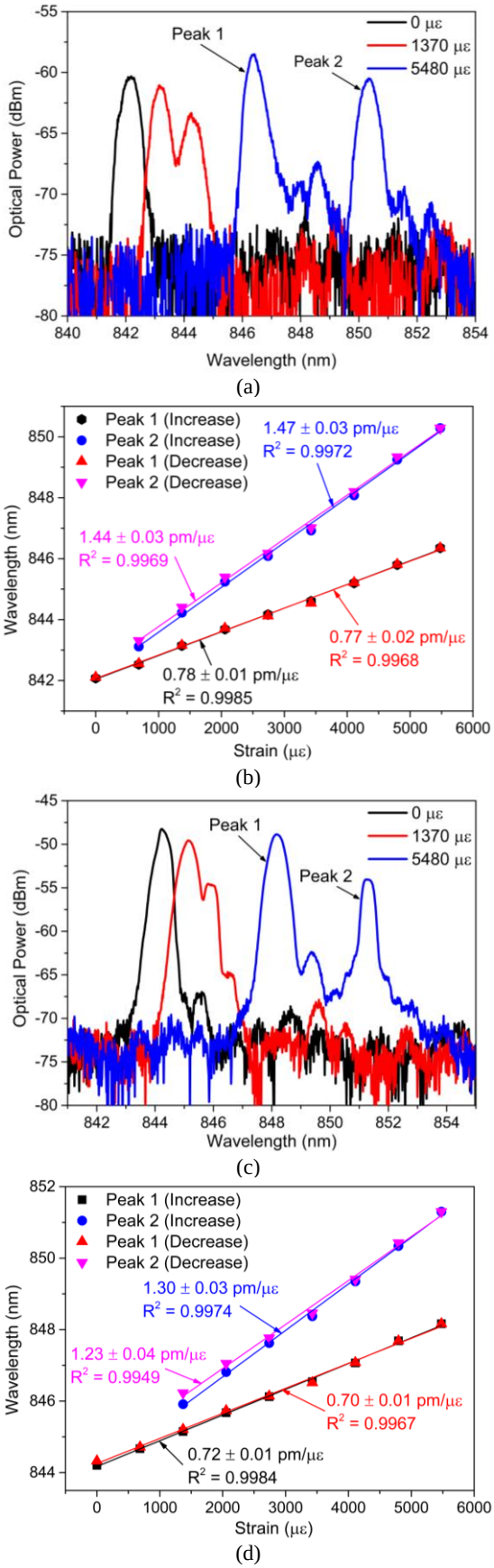

Fig. 6. (a) Reflection spectra of the POFBG 1 at different strain levels. (b) POFBG 1 wavelengths tuning with increasing/decreasing strain. (c) Reflection spectra of the POFBG 2 at different strains. (d) POFBG 2 wavelengths tuning with increasing/decreasing strain.

0733-8724 (c) 2020 IEEE. Personal use is permitted, but republication/redistribution requires IEEE permission. See http://www.ieee.org/publications_standards/publications/rights/index.html for more information.
Authorized licensed use limited to: Danmarks Tekniske Informationscenter. Downloaded on January 06,2021 at 06:06:43 UTC from IEEE Xplore. Restrictions apply.

This article has been accepted for publication in a future issue of this journal, but has not been fully edited. Content may change prior to final publication. Citation information: DOI 10.1109/JLT.2020.3046077, Journal of Lightwave Technology

TABLE I
STRAIN SENSITIVITIES AND MAXIMUM HYSTERESIS DURING DIFFERENT STRAIN CYCLES FOR POFBG 1 AND POFBG 2.

	Strain sensitivities	Peak 1 (pm/με)	Peak 2 (pm/με)	Maximum hysteresis (pm)
		Increase/Decrease		Peak 1/Peak 2
POFBG 1	Cycle 1 ≤ 3430 με	0.73/0.73	1.43/1.43	60/45
	Cycle 2 ≤ 5480 με	0.78/0.77	1.47/1.44	60/195
	Cycle 3 ≤ 6850 με	0.78/0.78	1.51/1.47	120/680
POFBG 2	Cycle 1 ≤ 3430 με	0.76/0.75	1.31/1.32	45/25
	Cycle 2 ≤ 5480 με	0.72/0.70	1.30/1.23	120/315
	Cycle 3 ≤ 6850 με	0.78/0.77	1.32/1.31	90/450

temperatures (25 ºC and 45 ºC), respectively, and Fig. 7 (b) and 7 (d) the central resonant wavelength of POFBG 1 and POFBG 2 shift with temperature, respectively. The obtained thermal sensitivities after applying a linear fit to the data of POFBG 1 were -79 ± 2 pm/ºC (increasing temperature) and -76 ± 2 pm/ºC (decreasing temperature), and for POFBG 2 were -81 ± 4 pm/ºC (increasing temperature) and -78 ± 4 pm/ºC (decreasing temperature). The hysteresis level during the thermal tests was 60 pm for both POFBG devices. During the temperature tests, reflection spectra showed just one peak for both gratings (see Fig. 7). Nevertheless, the sensitivities values obtained are approximately twice the thermal sensitivity value obtained for a POFBG in the same undoped mPOF without the micromachined slots (-39 ± 2 pm/ºC) [31]. These higher thermal sensitivity values can be in part explained by the absence of humidity control during the temperature tests. In addition, it can be assumed that the modulus of the sum between the thermal expansion coefficient and the thermo-optic coefficient increased in the grating region (due to the thermal expansion coefficient decrease and/or thermo-optic coefficient increase), leading to a higher negative thermal sensitivity of the POFBGs.

C. Humidity Response

The Relative Humidity (RH) characterization of the POFBGs was performed using a climate chamber (Angelantoni CHALLENGE 340), with 0.1 %RH resolution, at a constant temperature of 25 ºC. The POFBGs response were characterized by increasing the RH from 20 % to 80 %, and then decreased back to 20 %, using steps of 15 %. In each step, the environmental conditions inside the chamber were kept stable for 60 minutes. Fig. 8 (a) and 8 (c) show the central wavelength shift with the RH during the humidity test for POFBG 1 and POFBG 2, respectively. The central wavelength shift with the increasing/decreasing RH for POFBG 1 is shown in Fig. 8 (b), and the obtained sensitivities were 30.4 ± 0.5 pm/%RH and 29.6 ± 0.3 pm/%RH, respectively, with a hysteresis level of 80 pm. Fig. 8 (d) shows the response of the central wavelength from POFBG 2 to the increase/decrease of RH, and the obtained sensitivities were 30.7 ± 0.6 pm/%RH and 30.7 ± 0.5 pm/%RH, respectively, with a hysteresis level of 20 pm. These sensitivity values are similar to the ones obtained for a POFBG in the same

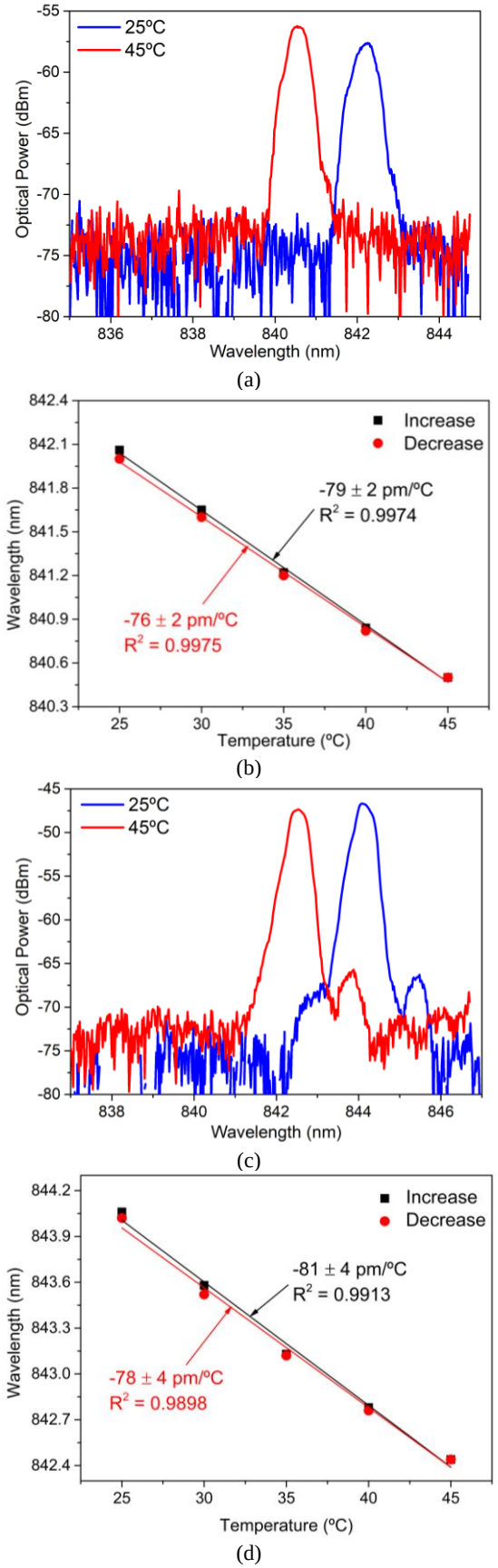

Fig. 7. (a) Reflection spectra of the POFBG 1 at different temperature levels. (b) POFBG 1 wavelength shift with increasing/decreasing temperature. (c) Reflection spectra of the POFBG 2 at different temperatures. (d) POFBG 2 wavelength shift with increasing/decreasing temperatures.

0733-8724 (c) 2020 IEEE. Personal use is permitted, but republication/redistribution requires IEEE permission. See http://www.ieee.org/publications_standards/publications/rights/index.html for more information.
Authorized licensed use limited to: Danmarks Tekniske Informationscenter. Downloaded on January 06,2021 at 06:06:43 UTC from IEEE Xplore. Restrictions apply.

This article has been accepted for publication in a future issue of this journal, but has not been fully edited. Content may change prior to final publication. Citation information: DOI 10.1109/JLT.2020.3046077, Journal of Lightwave Technology

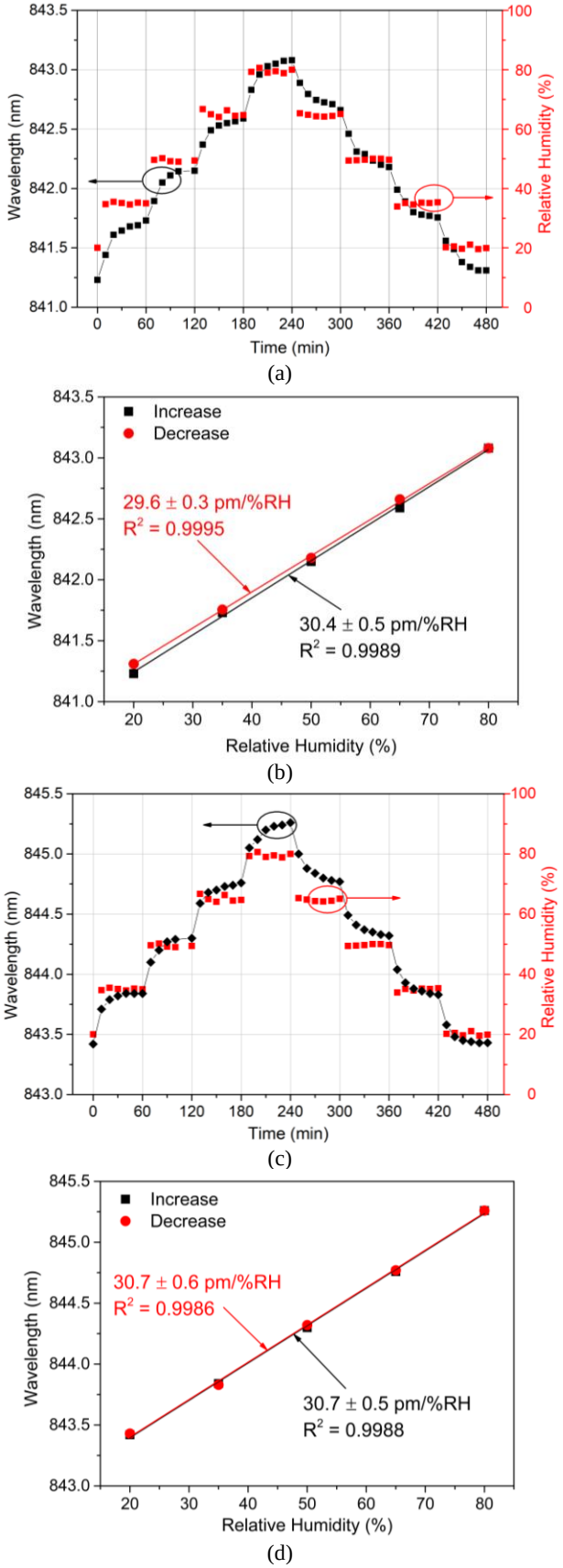

Fig. 8. (a) Bragg wavelength shift of the POFBG 1 and RH monitoring during the humidity test. (b) POFBG 1 wavelength shift with increasing/decreasing RH. (c) Bragg wavelength shift of the POFBG 2 and RH monitoring during the humidity test. (d) POFBG 2 wavelength shift with increasing/decreasing RH.

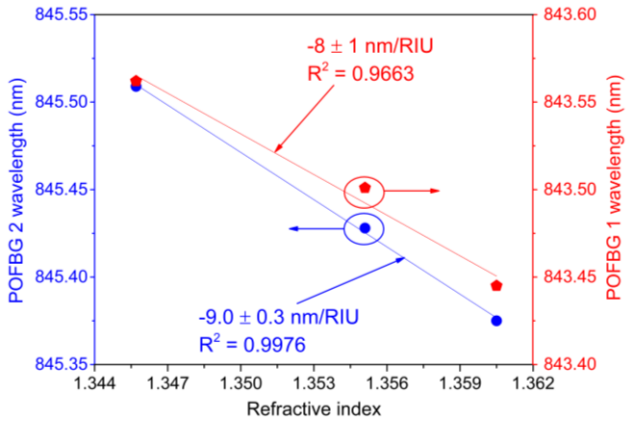

Fig. 9. Wavelength shift of the POFBG 1 (red) and POFBG 2 (blue) with increasing external refractive index.

mPOF without the micromachined slots (30 ± 5 pm/%RH) [31], showing that these structures in the POFBG do not affect the RH sensitivity, but are able to significantly reduce the response time. The humidity test showed again that the POFBGs spectrum profiles are identical to an uniform grating, showing just one peak during the entire experiment.

D. Refractive Index Response

A Refractive Index (RI) test was also performed to analyze the POFBGs response to this parameter. In this test, both POFBG devices were dipped into liquid containers filled with different RI solutions at room temperature (≈25 ºC). Three different solutions of water/ethanol (with different ethanol percentages) were used and the gratings were completely immersed in each one. In the beginning, both devices were immersed for 90 minutes in the first solution, with a measured RI of 1.3457, to ensure humidity and RI stabilization. The stabilization time for the other two solutions was 30 minutes, and during the RI test the POFBGs were kept unstrained. Fig. 9 shows the central wavelength shift with the increasing RI (up to 1.3605) for POFBG 1 and POFBG 2, and the obtained sensitivities were -8 ± 1 nm/RIU and -9.0 ± 0.3 nm/RIU, respectively. These results indicate that POFBG 2 has a better performance for RI monitoring, possibly due to the higher length of the micromachined slot (which covers approximately half the grating length), indicating that these microstructures increase the sensitivity and linearity to RI measurement (see Fig. 9).

IV. Strain and Temperature Simultaneous Measurement

Due to the dual-strain sensitivity of both POFBGs, with a single grating it was possible to simultaneously monitor strain and temperature variations. Since both POFBGs have two different strain responses and only one response to temperature changes, by using the mean value of the sensitivity coefficients for thermal variations and the mean values of the strain sensitivity coefficients, obtained during the 3 testing cycles for peaks 1 and 2, (2) can be rewritten as:

0733-8724 (c) 2020 IEEE. Personal use is permitted, but republication/redistribution requires IEEE permission. See http://www.ieee.org/publications_standards/publications/rights/index.html for more information.
Authorized licensed use limited to: Danmarks Tekniske Informationscenter. Downloaded on January 06,2021 at 06:06:43 UTC from IEEE Xplore. Restrictions apply.

This article has been accepted for publication in a future issue of this journal, but has not been fully edited. Content may change prior to final publication. Citation information: DOI 10.1109/JLT.2020.3046077, Journal of Lightwave Technology

$$\begin{bmatrix}\Delta\varepsilon\\ \Delta T\end{bmatrix}=\begin{bmatrix}-1.4358 & 1.4358\\ -0.0272 & 0.0142\end{bmatrix}\begin{bmatrix}\Delta\lambda_1\\ \Delta\lambda_2\end{bmatrix} \quad (3)$$

for POFBG 1, and:

$$\begin{bmatrix}\Delta\varepsilon\\ \Delta T\end{bmatrix}=\begin{bmatrix}-1.8060 & 1.8060\\ -0.0295 & 0.0169\end{bmatrix}\begin{bmatrix}\Delta\lambda_1\\ \Delta\lambda_2\end{bmatrix} \quad (4)$$

for POFBG 2. To demonstrate the sensing performance of the POFBGs, these devices underwent through relative strain variations from 700 με to 2100 με for POFBG 1 and from 980 με to 2380 με for POFBG 2, with steps about 280 με, at a constant temperature of 36 ºC. The reason to use relative strain values above 700 με and 980 με was to enable performance assessment of both peaks for each POFBG. The initial conditions were $\Delta\lambda_1$=0 and $\Delta\lambda_2$=0 for a temperature of 25 ºC and 0 % of applied strain. This test started by increasing the temperature from 25 ºC to 36 ºC (stabilization time of 30 minutes), followed by increasing the strain up to 2100 με and 2380 με for POFBG 1 and POFBG 2, respectively. A complementary test using the same initial conditions was performed, where the applied strain was kept constant at 1370 με and the temperature varied from 25 ºC up to 36 ºC, using 2 ºC steps (note that initially the temperature increased from 25 ºC to 26 ºC, first measured point). During all these measurements, the stabilization time for strain and temperature changes was 1 minute and 5 minutes, respectively.

Fig. 10 (a) and 10 (b) show the behave of the POFBG 1 and the POFBG 2 devices, respectively, during these two tests, at a constant relative strain of 1370 με (red) and at constant temperature of 36 ºC (blue). The Root Mean Square Errors (RMSEs) and the maximum deviation values for strain and temperature during these tests are summarized in Table II. The results are acceptable in order to create a well-conditioned system and the highest error values for strain and temperature obtained during constant strain and 11 ºC range temperature variation are ±23 με and ±0.5 ºC, respectively, while for constant temperature and strain variation of 2380 με (POFBG 2) are ±46 με and ±0.3 ºC, respectively. Nevertheless, it should be noted that these values are meant to provide an analysis between the real values and the ones obtain by the POFBG devices to study the simultaneous response to strain and temperature. RMSEs are highly dependent on the sensitivity coefficients obtained for both POFBGs and, consequently, on the calculated values of the matrixes (3) and (4). The accuracy of the obtained sensitivities will determine the magnitude of the errors during the simultaneous measurement. Besides this, other factors may have influenced the error values, such as the absence of humidity control and the use of a custom tubular furnace, with 1 °C resolution, for temperature variations during simultaneous measurements, resulting in low thermal stability during the tests.

To test further the simultaneous measurement capabilities of the POFBG devices, another test was performed where both strain and temperature changes were applied. In this experiment, the initial conditions were $\Delta\lambda_1$=0 and $\Delta\lambda_2$=0 for a temperature of 25 ºC and 1000 με of applied relative strain, for both POFBGs, which allowed to monitor both peaks since the beginning of the test. The results are shown in Fig. 11, showing the performance of the POFBG devices to strain variations above 1000 με at temperatures between 25 ºC and 35 ºC. The RMSEs values for temperature and strain for POFBG 1 are 0.6 ºC and 52 με, respectively, and for POFBG 2 are 0.4 ºC and 32 με, respectively. The error values are on the same magnitude as the previous tests, showing that they are conditioned by the sensitivity accuracy and the testing conditions. Therefore, it is

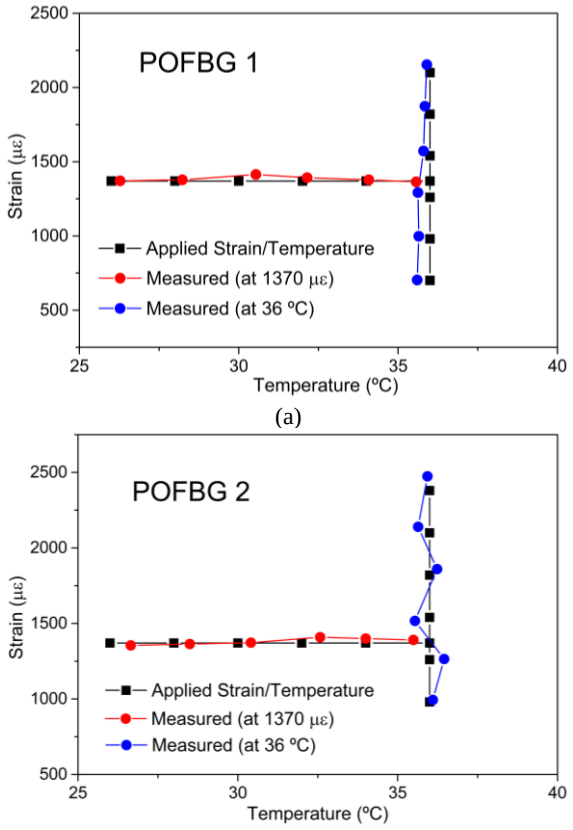

Fig. 10. Response to strain at a constant temperature (36 ºC) and to temperature at a constant strain (1370 με): (a) POFBG 1. (b) POFBG 2.

TABLE II
RMSE AND MAXIMUM DEVIATION VALUES FOR POFBG 1 AND POFBG 2 DURING STRAIN VARIATIONS AT 36 ºC AND TEMPERATURE VARIATIONS AT 1370 με

		RMSE		Maximum deviation	
		Strain (με)	Temperature (ºC)	Strain (με)	Temperature (ºC)
POFBG 1	At 36 ºC	37	0.3	54	0.4
	At 1370 με	21	0.3	44	0.5
POFBG 2	At 36 ºC	46	0.3	94	0.5
	At 1370 με	23	0.5	39	0.7

0733-8724 (c) 2020 IEEE. Personal use is permitted, but republication/redistribution requires IEEE permission. See http://www.ieee.org/publications_standards/publications/rights/index.html for more information.
Authorized licensed use limited to: Danmarks Tekniske Informationscenter. Downloaded on January 06,2021 at 06:06:43 UTC from IEEE Xplore. Restrictions apply.

This article has been accepted for publication in a future issue of this journal, but has not been fully edited. Content may change prior to final publication. Citation information: DOI 10.1109/JLT.2020.3046077, Journal of Lightwave Technology

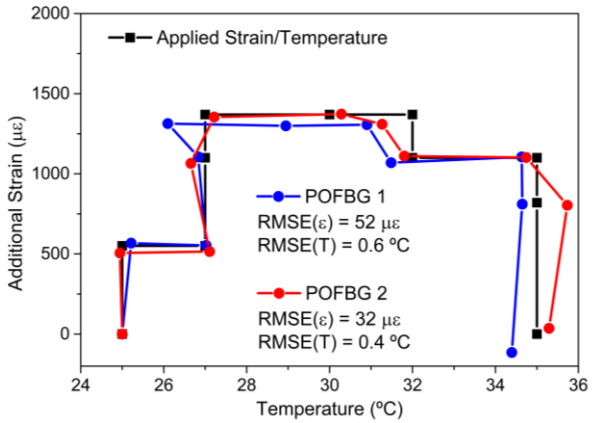

Fig. 11. POFGB devices response to different strain and temperature with the corresponding RMSEs values.

possible to lower the RMSEs by performing more sensing tests with higher resolution equipment. The results show that these sensors are a viable solution for applications where the simultaneous measurement of strain and temperature is required, and the obtained errors are acceptable. Besides the dual-sensitivity to strain, the main advantages of these POFBG devices when compared to other multiparameter sensors available are the use of a single grating and the non-addition of other materials on the fiber. These characteristics are of great importance to produce very compact size sensors for simultaneous measurements, with width and length values dependent on the fiber specification (usually micrometer scale) and grating characteristics (usually millimeter scale), respectively. Although the micromachined slots were produced by a femtosecond laser system in this work, the use of other laser systems or other diameter reduction techniques with lower costs, such as etching [56], may be possible, provided that the slots/diameter reduction precision is not compromised.

V. Conclusion

In conclusion, we demonstrate a novel technique for simultaneous measurement of strain and temperature, using just one FBG inscribed in a 2-rings undoped PMMA mPOF. Two different micromachined POFBG devices were produced by inscribing one FBG in each fiber with a UV laser, and then reducing the cross-section area in the grating region using a femtosecond laser system, achieving dual sensitivity to strain above a certain threshold. The mean values of the dual strain sensitivities obtained were 0.76 pm/με (peak 1, $0\ \mu\varepsilon \leq \varepsilon \leq 6850\ \mu\varepsilon$) and 1.46 pm/με (peak 2, $690\ \mu\varepsilon \leq \varepsilon \leq 6850\ \mu\varepsilon$) for POFBG 1, and for POFBG 2 the sensitivities were 0.75 pm/με (peak 1, $0\ \mu\varepsilon \leq \varepsilon \leq 6850\ \mu\varepsilon$) and 1.30 pm/με (peak 2, $960\ \mu\varepsilon \leq \varepsilon \leq 6850\ \mu\varepsilon$). On the other hand, during the thermal, humidity and refractive index tests, the POFBG devices behave like a uniform grating showing only one peak, with the mean sensitivity values of -77 pm/ºC and -80 pm/ºC for POFBG 1 and POFBG 2, respectively, which consists on a magnification by a factor of 2 when compared to a uniform POFBG in the same mPOF without the cross-section area reduction. Regarding the relative humidity sensitivity, the mean values obtained were 30.0 pm/%RH and 30.7 pm/%RH for POFBG 1 and POFBG 2, respectively, and for the refractive index characterization were obtained values of -8 ± 1 nm/RIU and -9.0 ± 0.3 nm/RIU for POFBG 1 and POFBG 2, respectively. To analyze the simultaneous measurement of both devices, two experiments were performed, one at constant temperature and another one at constant strain, resulting in a maximum RMSEs values of 0.3 ºC and 0.5 ºC (temperature) for POFBG 1 and POFBG 2, respectively, and 37 με and 46 με (strain) for POFBG 1 and POFBG 2, respectively. When changing both temperature and strain, the obtained RMSEs values were 0.6 ºC and 0.4 ºC (temperature) for POFBG 1 and POFBG 2, respectively, and 52 με and 32 με (strain) for POFBG 1 and POFBG 2, respectively. These results support that these devices are suitable for simultaneous measurement of temperature and strain, which could be a promising solution for sensing applications where simultaneous monitoring of strain and other parameters are crucial for a well-conditioned system. The use of just one grating for simultaneous measurements, without the need of adding other materials, is very promising to produce compact sensors (micrometer/millimeter scale) for *in situ* and *operando* applications. Furthermore, these devices may be used for other applications where phase-shift gratings are needed, using strain to tune the peaks spectral position and separation, according to the desired parameters. However, further tests must be conducted to analyze the impact of the fiber diameter reduction in the spectral characteristics of the gratings, when a high-power femtosecond laser is employed, since a refractive index modulation can occur at the focus spot and right after by filamentation [57].

References

[1] O. W. Ziemann, J. Krauser, P. E. Zamzow, and W. Daum, *POF Handbook*, 2nd ed., Berlin, Germany: Springer-Verlag, 2008.

[2] K. Peters, "Polymer optical fiber sensors—a review," *Smart Mater. Struct.*, vol. 20, no. 1, pp. 1-17, 2011.

[3] A. Leal-Junior *et al*., "Dynamic mechanical characterization with respect to temperature, humidity, frequency, and strain in mPOFs made of different materials," *Opt. Mater. Express*, vol. 8, no. 4, pp 804-815, 2018.

[4] Z. Xiong, G. D. Peng, B. Wu and P. L. Chu, "Highly tunable Bragg gratings in single-mode polymer optical fibers," *IEEE Photon. Technol. Lett*., vol. 11, no. 3, pp. 352-354, 1999.

[5] D. Webb and K. Kalli, "Polymer fiber Bragg gratings," in *Fiber Bragg Grating Sensors: Recent Advancements, Industrial Applications and Market Exploitation*, A. Cusano, A. Cutolo and J. Albert, Eds. Oak Park, IL: Bentham eBooks, pp. 292-312, 2011.

[6] A. Pospori, C. A. F. Marques, D. Sáez-Rodríguez, K. Nielsen, O. Bang, and D. J. Webb, "Thermal and chemical treatment of polymer optical fiber Bragg grating sensors for enhanced mechanical sensitivity," *Opt. Fiber Technol*., vol. 36, pp. 68-74, 2017.

[7] X. Chen, C. Zhang, D. J. Webb, K. Kalli, and G.-D. Peng, "Highly Sensitive Bend Sensor Based on Bragg Grating in Eccentric Core Polymer Fiber," *IEEE Photonics Technol. Lett*., vol. 22, no. 11, pp. 850-852, 2010.

[8] A. Stefani, S. Andresen, W. Yuan, N. Herholdt-Rasmussen and O. Bang, "High Sensitivity Polymer Optical Fiber-Bragg-Grating-Based Accelerometer," *IEEE Photonics Technol. Lett*., vol. 24, no. 9, pp. 763-765, 2012.

[9] C. A. F. Marques, G. D. Peng, and D. J. Webb, "Highly sensitive liquid level monitoring system utilizing polymer fiber Bragg gratings," *Opt. Express*, vol. 23, no. 5, pp. 6058-6072, 2015.

[10] M. Large, G. W. Barton, L. Poladian, and M. A. van Eijkelenborg, *Microstructured polymer optical fibre*, New York, NY, USA: Springer Science+Business Media LLC, 2008.

[11] G. Emiliyanov, P. E. Høiby, L. H. Pedersen, and O. Bang, "Selective serial multi-antibody biosensing with TOPAS microstructured polymer optical fibers," *Sensors*, vol. 13, no. 3, pp. 3242-3251, 2013.

[12] D. J. Webb, "Fibre Bragg grating sensors in polymer optical fibres," *Meas. Sci. Technol*., vol. 26, no. 9, pp. 1-11, 2015.

[13] G. D. Peng, Z. Xiong, and P. L. Chu, "Photosensitivity and Gratings in Dye-Doped Polymer Optical Fibers," *Opt. Fiber Technol*., vol. 5, no. 2,

0733-8724 (c) 2020 IEEE. Personal use is permitted, but republication/redistribution requires IEEE permission. See http://www.ieee.org/publications_standards/publications/rights/index.html for more information.
Authorized licensed use limited to: Danmarks Tekniske Informationscenter. Downloaded on January 06,2021 at 06:06:43 UTC from IEEE Xplore. Restrictions apply.

This article has been accepted for publication in a future issue of this journal, but has not been fully edited. Content may change prior to final publication. Citation information: DOI 10.1109/JLT.2020.3046077, Journal of Lightwave Technology

pp. 242-251, 1999.

[14] Z. Xiong, G. D. Peng, B. Wu, and P. L. Chu, "Highly tunable Bragg gratings in single-mode polymer optical fibers," *IEEE Photonics Technol. Lett*., vol. 11, no. 3, pp. 352-354, 1999.

[15] G. D. Peng and P. L. Chu, "Polymer Optical Fiber Photosensitivities and Highly Tunable Fiber Gratings," *Fiber Integr. Opt*., vol. 19, no. 4, pp. 277-293, 2000.

[16] R. Oliveira, L. Bilro, and R. Nogueira, "Bragg gratings in a few mode microstructured polymer optical fiber in less than 30 seconds," *Opt. Express*, vol. 23, no. 8, pp. 10181-10187, 2015.

[17] C. A. F. Marques, P. Antunes, P. Mergo, D. Webb, and P. Andre, "Chirped Bragg gratings in PMMA step-index polymer optical fiber," *IEEE Photonics Technol. Lett.*, vol. 29, no. 6, pp. 500-503, 2017.

[18] A. Pospori, C. A. F. Marques, O. Bang, D. J. Webb, and P. André, "Polymer optical fiber Bragg grating inscription with a single UV laser pulse," *Opt. Express*, vol. 25, no. 8, pp. 9028-9038, 2017.

[19] H. Dobb, D. J. Webb, K. Kalli, A. Argyros, M. C. J. Large and M. A. van Eijkelenborg, "Continuous wave ultraviolet light-induced fiber Bragg gratings in few- and single-moded microstructured polymer optical fibers," *Opt. Lett.*, vol. 30, pp. 3296-3298, 2005.

[20] I. P. Johnson, *et al*, "Optical fibre Bragg grating recorded in TOPAS cyclic olefin copolymer," *Electron. Lett*., vol. 47, no. 4, pp. 271-272, 2011.

[21] G. Woyessa, *et al*, "Single mode step-index polymer optical fiber for humidity insensitive high temperature fiber Bragg grating sensors," *Opt. Express*, vol. 24, no. 2, pp. 1253-1260, 2016.

[22] G. Woyessa, *et al*, "Zeonex microstructured polymer optical fiber: fabrication friendly fibers for high temperature and humidity insensitive Bragg grating sensing," *Opt. Mat. Express*, vol. 7, no. 1, pp. 286-295, 2017.

[23] G. Woyessa, *et al*, "Zeonex-PMMA microstructured polymer optical FBGs for simultaneous humidity and temperature sensing," *Opt. Lett*., vol. 42, no. 6, pp. 1161-1164, 2017.

[24] A. Fasano, *et al*, "Fabrication and characterization of polycarbonate microstructured polymer optical fibers for high-temperature-resistant fiber Bragg grating strain sensors," *Opt. Mat. Express*, vol. 6, no. 2, pp. 649-659, 2016.

[25] G. Woyessa, A. Fasano, C. Markos, H. K. Rasmussen and O. Bang, "Low loss polycarbonate polymer optical fiber for high temperature FBG humidity sensing," *IEEE Photon. Technol. Lett.*, vol. 29, no. 7, pp. 575-578, 2017.

[26] C. A. F. Marques *et al*., "Fast and stable gratings inscription in POFs made of different materials with pulsed 248 nm KrF laser," *Opt. Express*, vol. 26, no. 2, pp. 2013-2022, 2018.

[27] A. Lacraz, M. Polis, A. Theodosiou, C. Koutsides and K. Kalli, "Femtosecond laser inscribed Bragg gratings in low loss CYTOP polymer optical fiber," *IEEE Photon. Technol. Lett*., vol. 27, no. 7, pp. 693-696, 2015.

[28] R. Min, B. Ortega, A. Leal-Junior and C. Marques, "Fabrication and characterization of Bragg grating in CYTOP POF at 600-nm wavelength," *IEEE Sensors Lett*., vol. 2, no. 3, pp. 1-4, 2018.

[29] I.-L. Bundalo, K. Nielsen, C. Markos, and O. Bang, "Bragg grating writing in PMMA microstructured polymer optical fibers in less than 7 minutes," *Opt. Express*, vol. 22, no. 5, pp. 5270-5276, 2014.

[30] A. Stefani, M. Stecher, G. E. Town and O. Bang, "Direct Writing of Fiber Bragg Grating in Microstructured Polymer Optical Fiber," *IEEE Photonics Technol. Lett*., vol. 24, no. 13, pp. 1148-1150, 2012.

[31] R. Min *et al*., "Inscription of Bragg gratings in undoped PMMA mPOF with Nd:YAG laser at 266 nm wavelength," *Opt. Express*, vol. 27, no. 26, pp. 38039-38048, 2019.

[32] Y. Lou, Q. Zhang, H. Liu and G.-D. Peng, "Gratings fabrication in benzildimethylketal doped photosensitive polymer optical fibers using 355 nm nanosecond pulsed laser," *Opt. Lett.*, vol. 35, no. 5, pp. 751-753, 2010.

[33] D. Sáez-Rodríguez, K. Nielsen, H. K. Rasmussen, O. Bang and D. J. Webb, "Highly photosensitive polymethyl methacrylate microstructured polymer optical fiber with doped core," *Opt. Lett*., vol. 38, no. 19, pp. 3769-3772, 2013.

[34] L. M. Pereira *et al*., "Phase-shifted Bragg grating inscription in PMMA microstructured POF using 248 nm UV radiation," *J. Light. Technol.*, vol. 35, no.23, pp. 5176-5184, 2017.

[35] L. Pereira *et al*., "Polymer optical fiber Bragg grating inscription with a single Nd:YAG laser pulse," *Opt. Express*, vol. 26, no.14, pp. 18096-18104, 2018.

[36] X. Hu *et al*., "BDK-doped core microstructured PMMA optical fiber for effective Bragg grating photo-inscription," *Opt. Lett*., vol. 42, no. 11, pp. 2209-2212, 2017.

[37] U. Sampath, D. Kim, H. Kim and M. Song, "Polymer-coated FBG sensor for simultaneous temperature and strain monitoring in composite materials under cryogenic conditions," *Appl. Opt*., vol. 57, no. 3, pp. 492-497, 2018.

[38] P. Lu, L. Men and Q. Chen, "Polymer-Coated Fiber Bragg Grating Sensors for Simultaneous Monitoring of Soluble Analytes and Temperature," *IEEE Sensors Journal*, vol. 9, no. 4, pp. 340-345, 2009.

[39] C. Massaroni, M. A. Caponero, R. D´Amato, D. L. Presti and E. Schena, "Fiber Bragg Grating Measuring System for Simultaneous Monitoring of Temperature and Humidity in Mechanical Ventilation," *Sensors*, vol. 17, no. 4, 2017.

[40] M. Song, S. B. Lee, S. S. Choi and B. Lee, "Simultaneous Measurement of Temperature and Strain Using Two Fiber Bragg Gratings Embedded in a Glass Tube," *Opt. Fiber Technol*., vol. 3, pp. 194-196, 1997.

[41] E. Mesquita *et al*., "Optical sensors for bond-slip characterization and monitoring of RC structures," *Sensors and Actuators A: Physical*, vol. 280, pp. 332-339, 2018.

[42] S. W. James, M. I. Dockney and R. P. Tatam, "Simultaneous independent temperature and strain measurement using in-fibre Bragg grating sensors," *Electron. Lett*., vol. 32, no. 12, pp. 1133-1134, 1996.

[43] D. Pereira, O. Frazão and J. L. Santos, "Fiber Bragg grating sensing system for simultaneous measurement of salinity and temperature," *Opt. Engeneering*, vol. 43, no. 2, 2004.

[44] W. Yuan, A. Stefani and O. Bang, "Tunable polymer fiber Bragg grating (FBG) inscription: fabrication of dual-FBG temperature compensated polymer optical fiber strain sensors," *IEEE Photonic Technol. Lett*., vol. 24, no. 5, pp. 401-403, 2012.

[45] K. Bhowmik *et al*., "High intrinsic sensitivity etched polymer fiber Bragg grating pair for simultaneous strain and temperature measurements," *IEEE Sensors Journal*, vol. 16, no. 8, pp. 2453-2459, 2016.

[46] H. B. Liu, H. Y. Liu, G. D. Peng and P. L. Chu, "Strain and temperature sensor using a combination of polymer and silica fibre Bragg gratings," *Opt. Communications*, vol. 219, no. 16, pp. 139-142, 2003.

[47] A. G. Leal-Junior, C. Diaz, C. Marques, A. Frizera and M. J. Pontes, "3D-Printing Techniques on the Development of Multiparameter Sensors Using One FBG," *Sensors*, vol. 19, no. 16, 2019.

[48] A. K. Singh, S. Berggren, Y. Zhu, M. Han and H. Huang, "Simultaneous strain and temperature measurement using a single fiber Bragg grating embedded in a composite laminate," *Smart Mater. Struct.*, vol. 26, no. 11, 2017.

[49] T. Osuch, "Recent advances in tapered fiber Bragg grating technology and applications" in *17th Conference on Optical Fibres and Their Applications*, vol. 10325, Suprasl, Poland, 2017.

[50] K. Markowski, K. Jedrzejewski, M. Marzecki and T. Osuch, "Linearly chirped tapered fiber-Bragg-grating-based Fabry-Perot cavity and its application in simultaneous strain and temperature measurement," *Opt. Lett.*, vol. 42, no. 7, pp. 1464-1467, 2017.

[51] H. Z. Yang, X. G. Qiao, I. M. Rajibul, K. S. Lim and H. Ahmad, "Simultaneous measurement of aliphatic alcohol concentration and temperature based on etched taper FBG," *Sensors and Actuators B: Chemical*, vol. 202, pp. 959-963, 2014.

[52] D. Sáez-Rodríguez, R. Min, B. Ortega, K. Nielsen and D. J. Webb, "Passive and portable polymer optical fiber cleaver," *Photonics Technol. Lett*., vol. 28, no. 24, pp. 2834-2837, 2016.

[53] W. Yuan, *et al*, "Improved thermal and strain performance of annealed polymer optical fiber Bragg gratings," *Opt. Commun*., vol. 284, no. 1, pp. 176-182, 2011.

[54] G. Woyessa, K. Nielsen, A. Stefani, C. Markos and O. Bang, "Temperature insensitive hysteresis free highly sensitive polymer optical fiber Bragg grating humidity sensor," *Opt. Express*, vol. 24, no. 2, pp. 1206-1213, 2016.

[55] I.-L. Bundalo, K. Nielsen and O. Bang, "Angle dependent Fiber Bragg grating inscription in microstructured polymer optical fibers," *Opt. Express*, vol. 23, no. 3, pp. 3699-3707, 2015.

[56] R. Inglev , G. Woyessa, O. Bang and J. Janting, "Polymer Optical Fiber Modification by Etching using Hansen Solubility Parameters – A Case Study of TOPAS, Zeonex and PMMA," *J. Light. Technol*., vol. 37, no.18, pp. 4776-4783, 2019.

[57] S. L. Chin, *Femtosecond Laser Filamentation*, New York, USA: Springer-Verlag New York, 2010.

0733-8724 (c) 2020 IEEE. Personal use is permitted, but republication/redistribution requires IEEE permission. See http://www.ieee.org/publications_standards/publications/rights/index.html for more information.
Authorized licensed use limited to: Danmarks Tekniske Informationscenter. Downloaded on January 06,2021 at 06:06:43 UTC from IEEE Xplore. Restrictions apply.